



ELSEVIER

Contents lists available at [SciVerse ScienceDirect](http://www.sciencedirect.com)

## Comptes Rendus Physique

[www.sciencedirect.com](http://www.sciencedirect.com)

Structures and statistics of fluid turbulence / Structures et statistiques de la turbulence des fluides

Gross–Pitaevskii description of superfluid dynamics at finite temperature:  
A short review of recent results*Description Gross–Pitaevskii de la dynamique des superfluides à température finite :  
Une revue courte des résultats récents*

Marc Brachet

Laboratoire de physique statistique de l'École normale supérieure, associé au CNRS et aux Universités Paris VI et VII, 24, rue Lhomond, 75231 Paris cedex 05, France

## ARTICLE INFO

## Article history:

Available online 6 November 2012

## Keywords:

Turbulence  
Superfluidity  
Counterflow

## Mots-clés :

Turbulence  
Superfluidité  
Contre-écoulement

## ABSTRACT

The Gross–Pitaevskii equation (GPE) describes the dynamics of superflows and Bose–Einstein Condensates (BEC) at very low temperature. When a truncation of Fourier modes is performed, the resulting truncated GPE (TGPE) can also describe the correct thermal behavior of a Bose gas, as long as all relevant modes are highly occupied [M.J. Davis, S.A. Morgan, K. Burnett, Simulations of Bose fields at finite temperature, Phys. Rev. Lett. 87 (16) (2001) 160402]. We review some of our group's recent GPE- and TGPE-based numerical studies of superfluid dynamics and BEC stability. The relations with experiments are discussed.

© 2012 Académie des sciences. Published by Elsevier Masson SAS. All rights reserved.

## R É S U M É

L'équation de Gross–Pitaevskii (GPE) décrit la dynamique des superfluides et les condensats de Bose–Einstein (BEC) à très basse température. Quand une troncature des modes de Fourier est effectuée, l'équation résultante tronquée (TGPE) peut également décrire le comportement thermique correct d'un gaz de Bose, à condition que tous les modes concernés sont hautement occupés [M.J. Davis, S.A. Morgan, K. Burnett, Simulations of Bose fields at finite temperature, Phys. Rev. Lett. 87 (16) (2001) 160402]. Nous passons en revue quelques études numériques récentes faites par notre groupe, utilisant GPE et TGPE, de la dynamique des superfluides et de la stabilité des BEC. Les relations avec les expériences sont discutées.

© 2012 Académie des sciences. Published by Elsevier Masson SAS. All rights reserved.

## 1. Introduction

The present article is a review, summary and discussion of several of the results obtained, in the last 7 years or so in our group at ENS, by numerically studying the Gross–Pitaevskii equation (GPE) and also the so-called truncated (or Galerkin-projected) Gross–Pitaevskii equation (TGPE).

We first used direct numerical simulations (DNS) and branch-following methods to investigate the dynamics and stability of smooth solutions of the GPE. The present review follows a precedent review that was published in 2003 [1] in which the fields were always tacitly supposed to be smooth and spectrally-converged and thus the Gross–Pitaevskii equation

E-mail address: [brachet@lps.ens.fr](mailto:brachet@lps.ens.fr).

was considered as a partial differential equation (PDE). Since that period some progress was achieved within the same framework. We characterized the bifurcations of the 2D superflow around a cylinder using improved and very precise spectral methods based on mapped Chebyshev polynomials [2,3]. We also studied the sound emission produced by a pair of rotating vortices [4] and the dynamics of Kelvin waves [5].

More recently, we studied the equilibrium properties and the dynamics of the truncated Gross–Pitaevskii equation (TGPE), motivated by our results previously obtained on another system: the Fourier-truncated (or Galerkin-projected) dynamics of the 3D incompressible Euler equation. Indeed, this latter system is well-known to admit so-called absolute equilibrium solutions with Gaussian statistics and equipartition of kinetic energy among all Fourier modes [6–9]. Studying the relaxation dynamics of incompressible Euler-truncated system, we found that the thermalized modes between some transition wave number and the maximum wave number can act as a fictitious microworld providing an effective viscosity to the modes with wave numbers below the transition wave number [10]. We computed the effective viscosity [11] and also studied the effect of non-zero helicity [12] and generalized the notion of absolute equilibrium to classical compressible flows [13].

These results led us naturally to study the equilibrium properties and the dynamics of the TGPE, with the hope that it could provide us with a way to study finite-temperature effects such as dissipation and mutual friction. Note that several different theories of finite-temperature effects in BEC have been proposed and, at the moment, there is no consensus on the best model [14]. However, one of the proposed models is, indeed, the TGPE [15,14].

We clarified previous results concerning the nature of the phase transition that is present in the TGPE by showing that it is a standard second order transition [16]. Furthermore, we showed that the thermalization dynamics presents a dispersive bottleneck that slows down the thermalization in certain circumstances [17]. We also showed that most of the standard mutual-friction phenomenology does apply to the interaction of the vortices with the normal fluid that is present in the TGPE equilibrium. However, we found an exception to this agreement, due to an effect caused by the thermally induced Kelvin waves that produce an anomalous translational velocity for vortex rings [18]. This last result was found to depend only on the hydrodynamical effect of thermally-excited Kelvin waves. Note that such waves must also exist in physical superfluids such as low-temperature helium.

The article is organized as follows. Section 2 is devoted to the GPE and the stability of a superflow around a cylinder. Section 3 is devoted to the TGPE. The order of magnitude of the anomalous translational velocity for vortex rings in helium is discussed at the end of Section 3.4. Finally Section 4 is our conclusion.

## 2. Gross–Pitaevskii equation

### 2.1. Definitions of the system

Much work has been devoted to the determination of the critical velocity at which superfluidity breaks into a turbulent regime [19]. A mathematical model of superfluid  $^4\text{He}$ , valid at temperatures low enough for the normal fluid to be negligible, is the Gross–Pitaevskii equation [20–22]. In a related context, since dilute Bose–Einstein condensates (BEC) were produced experimentally [23–25], the dynamics of these compressible nonlinear quantum fluids has been accurately described by the GPE allowing direct quantitative comparison between theory and experiment [26].

Excitations of superfluid  $^4\text{He}$  are described by the famous Landau spectrum which includes phonons in the low wave number range, and maxons and rotons in the high (atomic-scale) wave number range. In contrast, the standard GPE (the equation used in the present paper) only has (dispersive) phonon excitations. It therefore incompletely represents the atomic-scale excitations in superfluid  $^4\text{He}$ . However, note that there exist generalizations of the GPE [27] that do reproduce the correct excitation spectrum, at the cost of introducing a spatially non-local nonlinear term. Note that further modifications to the nonlinear term also allow for obtaining any given density–pressure relation [1]. In this way a generalized GPE can be written with both the correct  $^4\text{He}$  equation of state and excitation spectrum.

However, for the sake of simplicity, we will work with the following simple form of the GPE, written with the physically relevant parameters: the coherence length  $\xi$  and the sound velocity  $c$  corresponding to unit density  $|\psi|^2 = 1$ .

$$i \frac{\partial \psi}{\partial t} = \frac{c}{\sqrt{2}\xi} [-\xi^2 \Delta \psi - \psi + |\psi|^2 \psi] \quad (1)$$

Several problems pertaining to superfluidity and BEC can thus be studied in the framework of Eq. (1). We now concentrate on the stability of a superflow in the presence of a moving obstacle [3].

### 2.2. Superflow past a disk

Following Ref. [3], the effect of a disk of radius unity (diameter  $D = 2$ ) moving at constant speed  $\mathbf{v} = v\mathbf{e}_x$  in a two-dimensional superfluid at rest is studied in the frame of the disk. This system is equivalent to a superflow around a disk, with constant speed  $-\mathbf{v}$  at infinity. Let  $\Omega$  be the plane  $\mathbb{C}$  deprived of  $\mathbb{D}$  the disk of radius unity and  $\partial\Omega$  the boundary of the domain, that is the circle of radius unity. The system can then be described with the following action functional:

$$A[\psi, \bar{\psi}] = \int dt \left\{ \sqrt{2}c\xi \int_{\Omega} d^2x \frac{i}{2} [\bar{\psi} \partial_t \psi - \psi \partial_t \bar{\psi}] - \mathcal{F}_0 \right\} \quad (2)$$

$\mathcal{F}_0$  is the energy of the system that reads

$$\mathcal{F}_0[\psi, \bar{\psi}] = \mathcal{E} - \mathbf{v} \cdot \mathcal{P} \quad (3)$$

with

$$\mathcal{E}[\psi, \bar{\psi}] = c^2 \int_{\Omega} d^2x \left[ \xi^2 |\nabla \psi|^2 + \frac{1}{2} (|\psi|^2 - 1)^2 \right] \quad (4)$$

$$\mathcal{P}[\psi, \bar{\psi}] = \sqrt{2} c \xi \int_{\Omega} d^2x \frac{i}{2} [(\psi - 1) \nabla \bar{\psi} - (\bar{\psi} - 1) \nabla \psi] \quad (5)$$

The presence of the constants  $-1$  in Eq. (5) ensures the convergence of the integral. The Euler–Lagrange equation corresponding to (2) is the following, slightly modified, GPE:

$$i \partial_t \psi = \frac{c}{\sqrt{2} \xi} [-\xi^2 \Delta \psi - \psi + |\psi|^2 \psi] + i \mathbf{v} \cdot \nabla \psi \quad (6)$$

defined in the domain  $\Omega$ . This equation can be mapped into two hydrodynamical equations by applying Madelung’s transformation [19]

$$\psi = \sqrt{\rho} \exp\left(\frac{i\phi}{\sqrt{2} c \xi}\right) \quad (7)$$

that defines a fluid of density  $\rho$  and velocity

$$\mathbf{U} = \nabla \phi - \mathbf{v} \quad (8)$$

The real and imaginary parts of the NLSE yield the following equations of motion:

$$\partial_t \rho + \nabla \cdot (\rho \mathbf{U}) = 0 \quad (9)$$

$$\partial_t \phi = -\frac{1}{2} (\nabla \phi)^2 + c^2 (1 - \rho) + c^2 \xi^2 \frac{\Delta \sqrt{\rho}}{\sqrt{\rho}} + \mathbf{v} \cdot \nabla \phi \quad (10)$$

Note that two non-dimensional parameters control the system: the Mach number  $\mathcal{M} = |\mathbf{v}|/c$  (where  $\mathbf{v}$  is the flow velocity at infinity) and the ratio of the healing length  $\xi$  to the diameter of the disk  $D$ .

In previous studies [28], boundary conditions were applied by adding to the GPE a repulsive potential term strong enough to force the density to zero inside the disk. Here, mathematically standard Dirichlet and Neumann boundary conditions will both be directly imposed at the border of the obstacle.

The Dirichlet boundary conditions read  $\psi|_{r=1} = 0$ . They thus prescribe zero density on the obstacle and correspond to the presence of an impenetrable obstacle (a laser in a BEC or a solid obstacle in superfluid  $^4\text{He}$ ). The condition on  $\rho$  is  $\rho = 0$  at  $r = 1$  and the square root of the density  $R = \sqrt{\rho}$  being constant on the obstacle, we have  $\partial_r R|_{r=1} = 0$  and  $\partial_\theta R|_{r=1} = 0$ . Using the continuity equation (9), it is easy to show that  $U_\perp = \partial_r \phi - v \cos \theta = 0$  at  $r = 1$ .

The Neumann boundary conditions read

$$\partial_r \rho = 0 \quad \text{at } r = 1 \quad (11)$$

$$U_\perp = \partial_r \phi - v \cos \theta = 0 \quad \text{at } r = 1 \quad (12)$$

and correspond to  $\psi$ :  $\partial_r (\psi \exp(\frac{i v r^2 \cos \theta}{\sqrt{2} c \xi r}))|_{r=r_0=1} = 0$ .

Note that, compared to the Dirichlet conditions, the Neumann conditions are more academic than physically realistic. However they correspond somewhat more closely to free-slip condition in standard compressible hydrodynamics.

### 2.3. Mapped Chebychev method

A code that can accurately accommodate both large- $r$  asymptotic behavior and thin boundary layers near the obstacle at  $r = 1$  was developed in Ref. [3] based on a Chebychev decomposition using an adequate mapping. The code describes a single obstacle, in contrast with periodic pseudo-spectral methods (previously used in Ref. [28]) which describe a periodic array of obstacles.

Using standard polar coordinates  $\{\theta, r\}$ , together with the relation

$$r(z) = z^{-1} \quad (13)$$

the domain  $\{0 \leq \theta < 2\pi, -1 \leq z \leq 1\}$ , can be mapped into the physical domain  $\{x, y\}$ , with  $x^2 + y^2 \geq 1$ .

The basic mapping is

$$x = z^{-1} \cos \theta, \quad y = z^{-1} \sin \theta \quad (14)$$

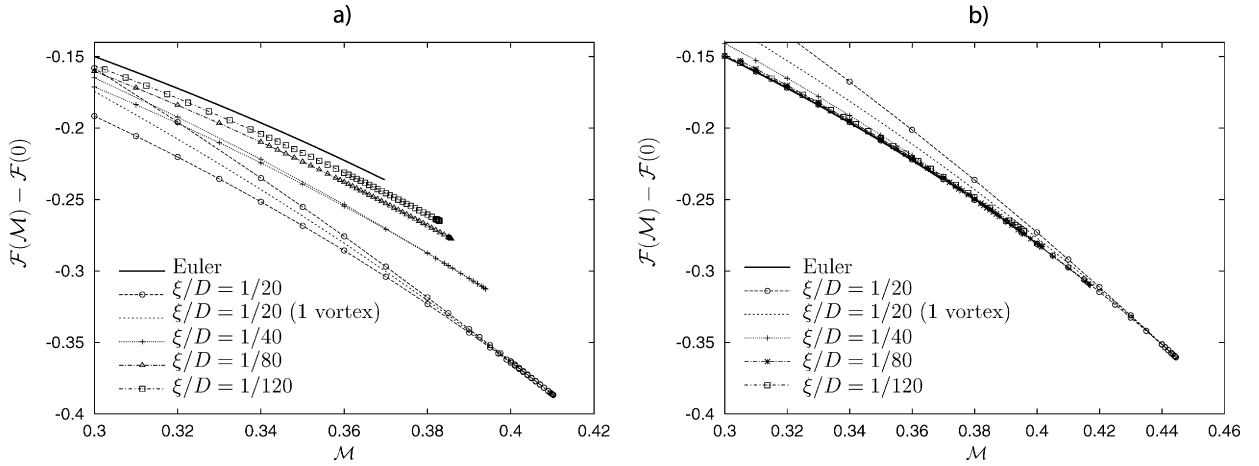


**Fig. 1.** Bifurcation diagrams for small coherence lengths. Energy functional  $\mathcal{F}(\mathcal{M}) - \mathcal{F}(0)$  versus Mach number. (a) Dirichlet conditions; (b) Neumann conditions. For  $\xi/D = 1/20$ , the asymmetric unstable solution branch is represented (it stands for a one-vortex branch stemming from a pitchfork bifurcation). At a fixed Mach number, the energy difference between a stable and an asymmetric unstable solution is roughly half the energy difference between a stable and a symmetric unstable solution.

and the inverse transformation reads

$$z = \pm \frac{1}{\sqrt{x^2 + y^2}}, \quad \theta = \arctan(y/x) + \frac{\pi \mp \pi}{2} \tag{15}$$

The equations of motion are expressed as partial differential equations in the  $\{\theta, z\}$  domain by writing the differential operators  $\nabla$  and  $\Delta$  in terms of  $\theta$  and  $z$  derivatives that are polynomial in  $z$ , e.g.,

$$\Delta \psi = z^2 \frac{\partial^2 \psi}{\partial \theta^2} + z^4 \frac{\partial^2 \psi}{\partial z^2} + z^3 \frac{\partial \psi}{\partial z}$$

The field  $\psi$  is then spatially discretized, in the  $(\theta, z)$  domain, using a standard Chebychev–Fourier pseudo-spectral method [29], based on the expansion

$$\psi(\theta, z) = \sum_{n=1-N_\theta/2}^{N_\theta/2} \left\{ \sum_{p=0}^{N_r} \psi_{n,p} T_p(z) \right\} \exp in\theta \tag{16}$$

where  $T_p(z) = \cos(p \arccos z)$  is the order- $p$  Chebychev polynomial and  $N_\theta$  and  $N_r$  represent resolutions.

In order to study bifurcation diagrams, one needs to define a new free energy by

$$\mathcal{F}[\psi, \bar{\psi}] = \mathcal{F}_0[\psi, \bar{\psi}] - \mathbf{v} \cdot \sqrt{2} c \xi \oint_{\partial \Omega} d\ell \mathbf{n} \frac{1}{2i} (\psi - \bar{\psi}) \tag{17}$$

which implies the existence of a generic cusp in  $\mathcal{F}$  at the bifurcation point (see Fig. 1).

#### 2.4. Numerical results

The values of  $\mathcal{F}(\mathcal{M}) - \mathcal{F}(0)$  are displayed in Fig. 1 as a function of the Mach number  $\mathcal{M}$  for various values of  $\xi/D$  and the two types of boundary conditions. As can be seen by inspection of the figure, for each  $\xi/D$ , the stable branch (solid line) disappears with the unstable solution (dashed line) at a saddle-node bifurcation when  $\mathcal{M} = \mathcal{M}_c$ . There are no stationary solutions beyond this point. This qualitative behavior is the signature of a Hamiltonian saddle-node bifurcation.

At a fixed Mach number, the energy difference between a stable and an unstable solution corresponds to the energy barrier necessary to dynamically nucleate an excitation. Note that this barrier for a symmetric unstable solution is about twice that of an asymmetric unstable solution.

Fig. 2 shows the density  $\rho = |\psi|^2$  of stationary symmetric unstable solutions  $\mathcal{M} = 0.3$  and  $\xi/D = 1/20$  for the two types of boundary conditions, obtained by a branch-following method that allows to also find unstable solutions. It is apparent by inspection of the figure that the symmetric unstable branch corresponds to a two-vortex solution.

For Dirichlet boundary conditions, similar results were found with periodic pseudo-spectral codes [28]. However, the new method directly imposes the correct boundary conditions without resorting to an artificial repulsive potential. Also note that the critical Mach number is here determined for a single obstacle, whereas a periodic array of obstacles was used previously.

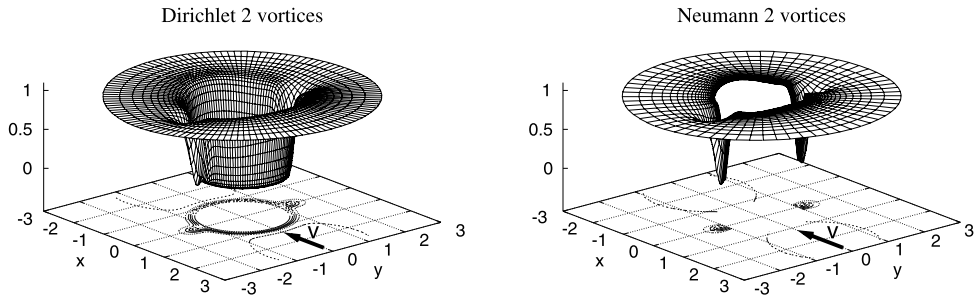


**Fig. 2.** Density  $\rho = |\psi|^2$  of stationary symmetric unstable solutions for  $\xi/D = 1/20$  and  $\mathcal{M} = 0.3$  far from the bifurcation threshold. Left: Dirichlet conditions; right: Neumann conditions.

### 3. Spectrally truncated Gross–Pitaevskii equation

Following Refs. [16–18], we now turn to the TGPE and finite-temperature effects.

#### 3.1. Definitions of the system

The TGPE is obtained from the GPE by simply truncating the Fourier transform of the wavefunction  $\psi$ :  $\hat{\psi}_{\mathbf{k}} \equiv 0$  for  $|\mathbf{k}| > k_{\max}$  [15,14]. Introducing the Galerkin projector  $\mathcal{P}_G$  that reads in Fourier space  $\mathcal{P}_G[\hat{\psi}_{\mathbf{k}}] = \theta(k_{\max} - |\mathbf{k}|)\hat{\psi}_{\mathbf{k}}$  with the Heaviside function  $\theta(\cdot)$ , the TGPE explicitly reads

$$i\hbar \frac{\partial \psi}{\partial t} = \mathcal{P}_G \left[ -\frac{\hbar^2}{2m} \nabla^2 \psi + g \mathcal{P}_G[|\psi|^2] \psi \right] \quad (18)$$

where  $m$  is the mass of the condensed particles and  $g = 4\pi\tilde{a}\hbar^2/m$ , with the  $s$ -wave scattering length  $\tilde{a}$ . Madelung's transformation

$$\psi(\mathbf{x}, t) = \sqrt{\frac{\rho(\mathbf{x}, t)}{m}} \exp \left[ i \frac{m}{\hbar} \phi(\mathbf{x}, t) \right]$$

relates the (complex) wavefunction  $\psi$  to a superfluid of density  $\rho(\mathbf{x}, t)$  and velocity  $\mathbf{v} = \nabla\phi$ , where  $\hbar/m$  is the Onsager–Feynman quantum of velocity circulation around the  $\psi = 0$  vortex lines [14]. When Eq. (18) is linearized around a constant  $\psi = \hat{\psi}_0$ , the sound velocity is given by  $c = (g|\hat{\psi}_0|^2/m)^{1/2}$  with dispersive effects taking place at length scales smaller than the coherence length  $\xi = (\hbar^2/2m|\hat{\psi}_0|^2g)^{1/2}$  that also corresponds to the vortex core size. In the TGPE numerical simulations presented here the density  $\rho = mN/V$  is fixed to 1 and the physical constants in Eq. (18) are determined by the values of  $\xi k_{\max}$  and  $c = 2$ . The quantum of circulation  $h/m$  has the value  $c\xi/\sqrt{2}$  and  $V = (2\pi)^3$ .

Eq. (18) exactly conserves the energy

$$H = \int d^3x \left( \frac{\hbar^2}{2m} |\nabla\psi|^2 + \frac{g}{2} [\mathcal{P}_G|\psi|^2]^2 \right)$$

and the number of particles

$$N = \int d^3x |\psi|^2$$

Using Fourier pseudo-spectral methods the momentum  $\mathbf{P} = \frac{i\hbar}{2} \int d^3x (\psi \nabla \bar{\psi} - \bar{\psi} \nabla \psi)$  is also conserved with dealiasing performed by the 2/3-rule ( $k_{\max} = 2/3 \times M/2$  [29] at resolution  $M$ ).

#### 3.2. Absolute equilibrium and second order phase transition

The discovery of the phase transition present in the microcanonical equilibrium of the TGPE has a somewhat convoluted story. Davis et al. [15] first considered random initial data defined in Fourier space by modes with constant modulus and random phases up to some maximum wavenumber (determined by the energy). They found that the numerical evolution of the TGPE reached (microcanonical) equilibrium and that a condensation transition of the equilibrium was obtained when the initial-data energy was varied.

The same condensation transition was later studied by Connaughton et al. [30] and interpreted as a condensation of classical nonlinear waves. Using a modified wave turbulence theory with ultraviolet cutoff, they argued that the transition to condensation should be subcritical. They found their theory in quantitative agreement with numerical integration of the GPE, using the same stochastic initial conditions than those of Ref. [15]. However, the authors later argued that, as weak

turbulence theory is expected to breakdown nearby the transition to condensation, the subcritical nature of the transition predicted by their theory was not physical [31].

Microcanonical equilibrium states were thus well-known to result from long-time integration of TGPE [15,30,32]. In this context, we reflected upon the analogy of the TGPE with classical truncated systems, such as the truncated Euler equation, that are known to admit absolute equilibrium solutions with Gaussian statistics and equipartition of kinetic energy among all Fourier modes [6–9].

This analogy led us to consider [16] grand canonical states that are given by the probability distribution

$$\mathbb{P}_{\text{st}}[\psi] = \mathcal{Z}^{-1} \exp[-\beta(H - \mu N - \mathbf{v}_n \cdot \mathbf{P})] \quad (19)$$

They allow to directly control the temperature (instead of the energy in a microcanonical framework). These states are not Gaussian because of the quartic character of  $H$  (see above). However, they can be efficiently obtained by constructing a stochastic process that converges to a realization with the probability  $\mathbb{P}_{\text{st}}[\psi]$  [13]. This process is simply a nonlinear diffusion equation with noise. It is formally defined by a Langevin equation consisting in a stochastic Ginzburg–Landau equation (SGLE):

$$\hbar \frac{\partial \psi}{\partial t} = \mathcal{P}_G \left[ \frac{\hbar^2}{2m} \nabla^2 \psi - g \mathcal{P}_G[|\psi|^2] \psi \right] + \mathcal{P}_G[\mu \psi - i \hbar \mathbf{v}_n \cdot \nabla \psi] + \sqrt{\frac{2\hbar}{V\beta}} \mathcal{P}_G[\zeta(\mathbf{x}, t)] \quad (20)$$

where the white noise  $\zeta(\mathbf{x}, t)$  satisfies  $\langle \zeta(\mathbf{x}, t) \zeta^*(\mathbf{x}', t') \rangle = \delta(t - t') \delta(\mathbf{x} - \mathbf{x}')$ ,  $\beta$  is the inverse temperature,  $\mu$  is the chemical potential and  $\mathbf{v}_n$  is the normal velocity. The term  $i \hbar \mathbf{v}_n \cdot \nabla \psi$  induces an asymmetry in the repartition of sound waves and generates non-zero momentum states. These states do not generally correspond to a condensate moving at velocity  $\mathbf{v}_s = \mathbf{v}_n$  because  $\mathbf{v}_s$  is the gradient of a phase and takes discrete values for finite size systems. Equilibrium states with non-zero values of the counterflow  $\mathbf{w} = \mathbf{v}_n - \mathbf{v}_s$  can be generated in this way.

Using this algorithm in [16] the microcanonical and grand canonical ensembles were shown to be equivalent and the condensation transition reported in [15,30] identified with the standard second order  $\lambda$ -transition. Indeed, the  $(\mathbf{v}_n = 0)$  statistic weight of distribution (19) exactly corresponds to that of (standard two-component) second order phase transitions [33,34]. The condensation transition must thus be in this standard universality class.

### 3.3. Dispersive bottleneck

Motivated by the spontaneous thermalization of the truncated Euler dynamics [10], we now study the equivalent TGPE problem by making use of the so-called superfluid Taylor–Green (TG) vortex [1]. The TGPE integrations are performed with a dedicated pseudo-spectral code that uses the symmetries to speed up computations (see Refs. [35,36]). Up to  $512^3$  collocation points are used and the coherence length is determined by  $\xi k_{\text{max}} = 1.48$ . To study this relaxation dynamics, we express the energy per unit volume  $E_{\text{tot}} = (H - mc^2 N)/V + \frac{mc^2}{2}$  as the sum of three (space-averaged) parts [35,36]: the kinetic energy  $E_{\text{kin}} = \langle 1/2(\sqrt{\rho} v_j)^2 \rangle$ , the internal energy  $E_{\text{int}} = \langle (c^2/2)(\rho - 1)^2 \rangle$  and the quantum energy  $E_q = \langle c^2 \xi^2 (\partial_j \sqrt{\rho})^2 \rangle$ . Parseval's theorem allows to define corresponding energy spectra: e.g. the kinetic energy spectrum  $E_{\text{kin}}(k)$  as the (solid angle) integral of  $|\frac{1}{2(2\pi)^3} \int d^3 r e^{i r_j k_j} \sqrt{\rho} v_j|^2$ .  $E_{\text{kin}}(k)$  can be further decomposed into compressible  $E_{\text{kin}}^c(k)$  and incompressible  $E_{\text{kin}}^i(k)$  parts, using  $(\sqrt{\rho} v_j) = (\sqrt{\rho} v_j)^c + (\sqrt{\rho} v_j)^i$  with  $\nabla \cdot (\sqrt{\rho} v_j)^i = 0$ . The temporal evolution of  $E_{\text{kin}}$ ,  $E_{\text{kin}}^i$ ,  $E_{\text{kin}}^c$ ,  $E_q + E_{\text{int}}$  is displayed in Fig. 3(a) and the corresponding energy spectra in Fig. 3(c–d).

Three evolution phases are apparent from Fig. 3(a). The first phase, for  $t \lesssim 15$ , corresponds to the GPE regime previously studied in [35,36]. In the second phase, for  $20 \lesssim t \lesssim 70$ , the spectral convergence of the GP partial differential equation is lost and the dynamics is influenced by  $k_{\text{max}}$ . Partial thermalization starts to take place at large wavenumbers where  $E_{\text{kin}}(k) \sim k^2$  (see Fig. 3(c)). Fig. 3(b) shows that this phase is delayed when the resolution is increased at constant  $\xi k_{\text{max}}$ . When  $t > 80$  the system reaches the thermodynamic equilibrium with equipartition of energy between  $E_{\text{kin}}^c$  and  $E_q + E_{\text{int}}$ , see Fig. 3(d). Finally,  $E_{\text{kin}}^i$  vanishes before final thermalization (see Fig. 3(a–b)). Similar relaxation mechanisms are also present in the truncated Euler dynamics [10]. Note that Salort, Roche and L ev eque [37], using a “truncated HVBK” model, also obtained equipartition of kinetic energy in quantum turbulence with a characteristic  $k^2$  velocity spectrum.

We now turn to the study of dispersive effects on the thermalization of the TGPE dynamics. In order to investigate dispersive effects, the TG initial condition described above is prepared at fixed  $\xi = \sqrt{2}/20$  and varying resolution:  $64^3$ ,  $128^3$  and  $256^3$ . The three initial conditions thus represent the same field at different resolutions and thus different  $k_{\text{max}}$ .

The evolutions of the energies of the three runs are shown in Fig. 4(a). They are identical until  $t \approx 5$  where the run at resolution  $64^3$  starts to lose spectral convergence. All runs appear to have completely thermalized at  $t \approx 20$ . However the kinetic energy spectrum corresponding to this time, displayed in Fig. 4(b), shows clear differences between runs. The high-wavenumber modes are thermalized in the  $64^3$  run but they decay at large- $k$  at higher resolutions. In the  $256^3$  run, two zones are clearly distinguished: an intermediate thermalized range (with approximative  $k^2$  scaling) followed, well before  $k_{\text{max}} = 85$ , by a steep decay zone.

The temporal evolution of  $E_{\text{kin}}(k)$  for the  $256^3$  run displayed in Fig. 4(c) is well represented by a fit of the form  $A(t)k^2 \exp[-\gamma^2(t)k^2]$ , where  $A(t)$  and  $k_c(t) \sim \gamma^{-1}(t) \ll k_{\text{max}}$  are increasing functions of  $t$ . Such a behavior of the energy spectra ensures spectral convergence and the dynamics is thus not influenced by  $k_{\text{max}}$ .

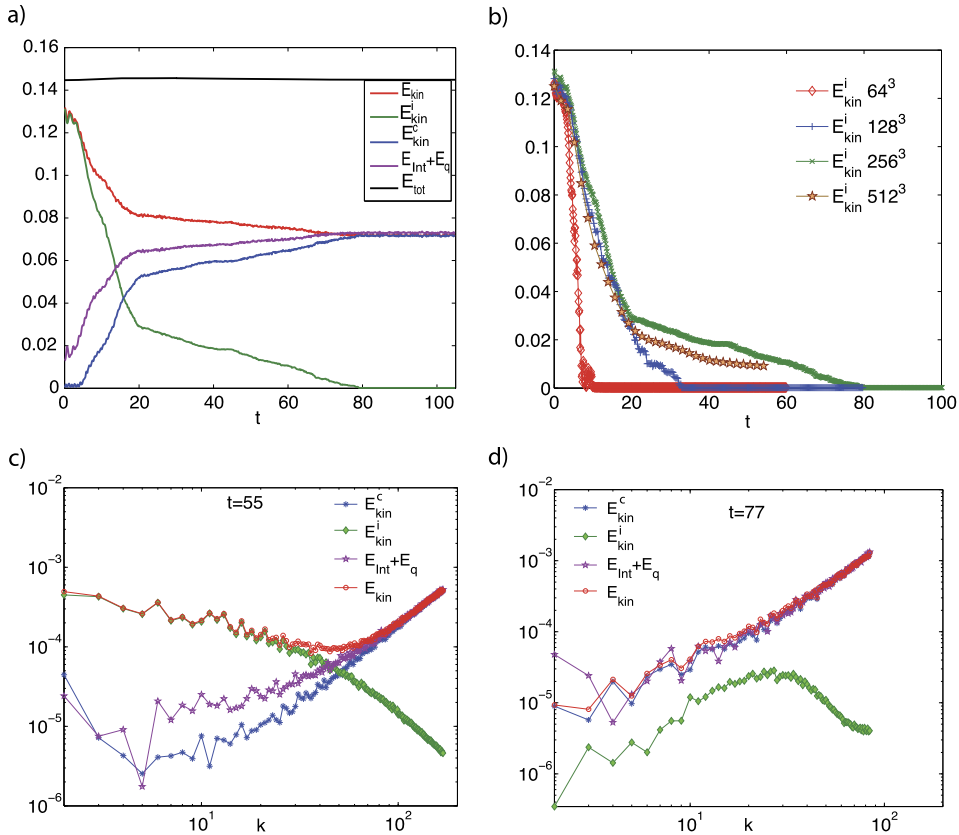


**Fig. 3.** (Color online.) (a) Temporal evolution of energies  $E_{kin}^c$ ,  $E_{kin}^i$ ,  $E_{kin}$  and  $E_q + E_{int}$ . At large times, the incompressible energy vanishes and equipartition of energy between  $E_{kin}$  and  $E_q + E_{int}$  is observed. Resolution of  $256^3$ . (b) Temporal evolution of  $E_{kin}^i$  at resolution of  $64^3$ ,  $128^3$ ,  $256^3$  and  $512^3$  with constant  $\xi k_{max} = 1.48$ . (c-d) Energy spectra at  $t = 55$  and  $t = 77$  resolution  $512^3$  and  $256^3$  respectively.

This new regime can be described as a (quasi) thermalization, with self-truncation at wavenumber  $k_c$  and temperature  $T \sim E/k_c^3$ , that spontaneously establishes itself within the GP partial differential equation dynamics when the direct energy cascade is inhibited by a dispersive bottleneck for the energy transfer.

An open question is whether thermalization is simply delayed or completely inhibited in the self-truncation regime  $\xi k_{max} \rightarrow \infty$ . It is not feasible now to directly study this limit, within the TG framework, as it requires long runs at arbitrarily high resolution. To skip the TG cascade regime and directly study the self-truncated thermalization regime we use initial data generated by the SGLE instead of the TG vortex. To wit, we use Eq. (20) with a variable truncation wavenumber  $k_c^{in}$ , set to a target value of  $k_c$ , smaller than the maximum truncation wavenumber  $k_{max}$  allowed by the resolution. This SGLE-generated initial data is then used to run the TGPE at a given value of  $\xi k_c$  with arbitrarily large values of  $\xi k_{max}$ .

A number of such runs were performed at resolution  $64^3$  with various values of  $k_c^{in}$ ,  $\xi$ , and initial energy  $E^{in}$ . The results of these computations are compared with the TG runs and displayed in Fig. 4(d). It is apparent from the figure that the self-truncation behavior is robust. Orders of magnitudes pertaining to physical BEC are discussed in Refs. [17,16].

### 3.4. Two-fluid effects and anomalous velocity of vortex rings

We now turn to the study of two-fluid effects. The direct control of the counterflow  $\mathbf{v}_n$  in the SGLE algorithm given in Section 3.2 allows to obtain the temperature dependence of  $\rho_n$  in the TGPE context.

In Ref. [18], the response to SGLE-generated counterflow of two types of vortex arrays (straight vortices and rings, generated using a Newton method) was compared with the prediction of the standard phenomenological model for the vortex line velocity  $\mathbf{v}_L$  [19]:

$$\mathbf{v}_L = \mathbf{v}_{sl} + \alpha \mathbf{s}' \times (\mathbf{v}_n - \mathbf{v}_{sl}) - \alpha' \mathbf{s}' \times [\mathbf{s}' \times (\mathbf{v}_n - \mathbf{v}_{sl})] \quad (21)$$

where  $\mathbf{s}'$  is the tangent of the vortex line,  $\mathbf{v}_{sl} = \mathbf{v}_s + \mathbf{u}_i$  is the local superfluid velocity with the self-induced vortex velocity  $\mathbf{u}_i$  and the normal velocity  $\mathbf{v}_n$ . The mutual-friction coefficients in Eq. (21) are typically written as  $\alpha = B \rho_n / 2\rho$ ,  $\alpha' = B' \rho_n / 2\rho$  where  $B$  and  $B'$  are order-one and weakly temperature-dependent. Eq. (21) applied to a straight vortex with  $\mathbf{v}_n$  perpendicular to the vortex and  $\mathbf{v}_s = 0$  yields  $\alpha' = v_{\parallel} / v_n$ , where  $v_{\parallel}$  denotes the induced velocity of the vortex line parallel to  $\mathbf{v}_n$ .

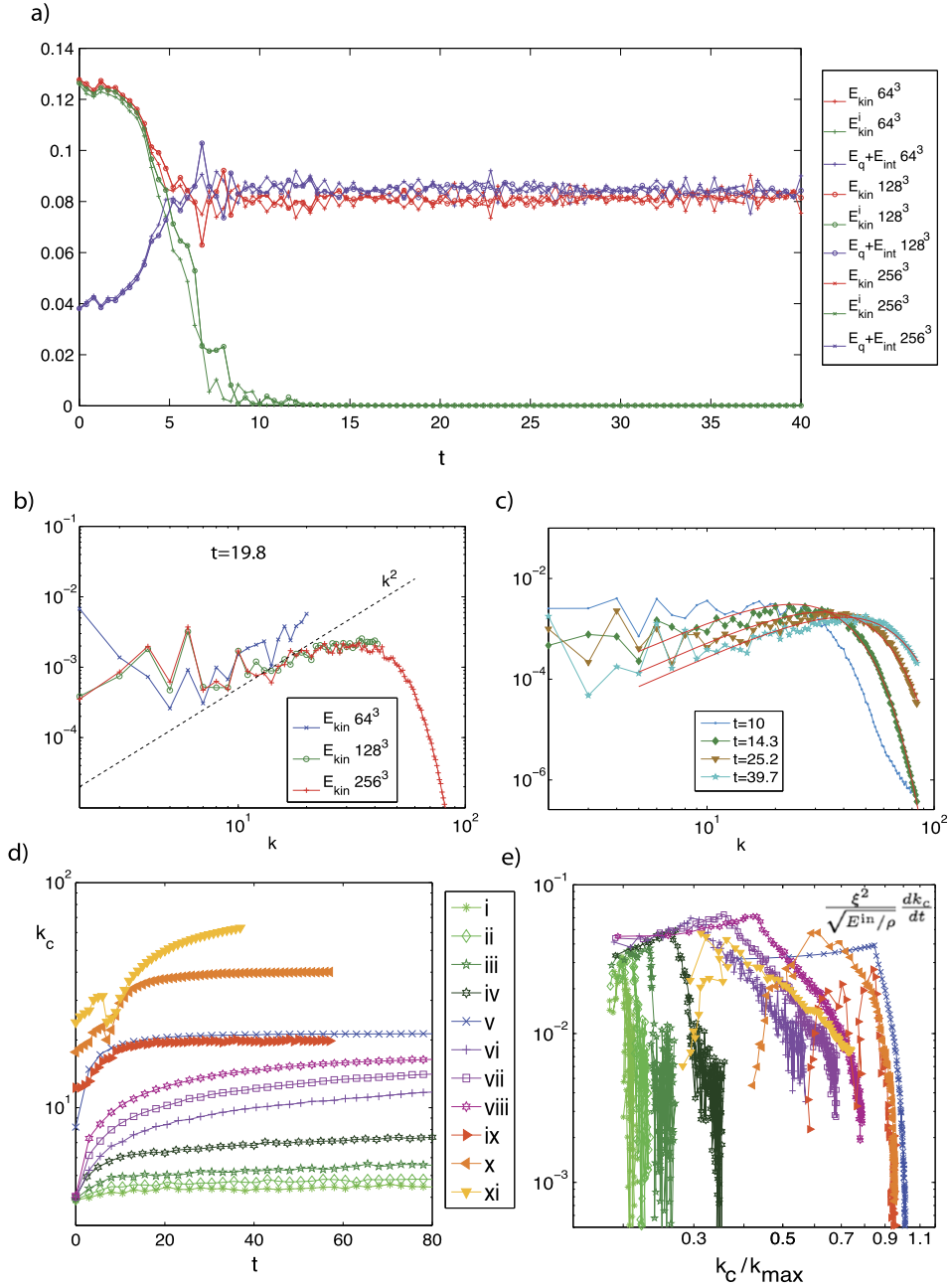


**Fig. 4.** (Color online.) (a) Evolution of energies at  $\xi = \sqrt{2}/20$  and resolution  $64^3$ ,  $128^3$  and  $256^3$ . (b) Energy spectrum  $E_{\text{kin}}(k)$  at  $t = 19.8$  for the three TG runs. (c) Evolution of  $E_{\text{kin}}(k)$ , solid red lines are fits of the form  $AK^2 \exp[-\gamma^2 k^2]$  (see text). (d) Evolution of  $k_c$ . Curves i–iv:  $\xi = 2\sqrt{2}/5$ ,  $k_c^{\text{in}} = 4$ ,  $E^{\text{in}} = 0.1, 0.2, 0.4, 1$ ; v:  $\xi = \sqrt{2}/10$ ,  $k_c^{\text{in}} = 8$ ,  $E^{\text{in}} = 0.2$ ; vi–viii:  $\xi = \sqrt{2}/5$ ,  $E^{\text{in}} = 0.1, 0.2, 0.4$  (i–viii in resolution  $64^3$ ); ix–xi: Taylor–Green resolutions  $64^3$ ,  $128^3$  and  $256^3$ . (e) Parametric representation  $dk_c/dt$  vs.  $k_c/k_{\text{max}}$  (same labels as (d)).

It was found in Ref. [18] that the straight vortex array was behaving consistently with standard phenomenology and reasonable (order unity) values for the constants  $B$  and  $B'$ .

We now turn to the interaction of vortex rings and counterflow. The Biot–Savart self-induced velocity of a perfectly circular vortex ring of radius  $R$  is given by

$$u_i = \frac{\hbar}{2m} \frac{C(R/\xi)}{R}, \quad C(z) = \ln(8z) - a \tag{22}$$

where  $a$  is a core model-dependent constant [19]. We have checked, using an initial data  $\psi_{\text{ring}}$  prepared by a Newton method that the GPE (large  $R/\xi$ ) ring translational velocity is well reproduced by (22) with  $a = 0.615$ .

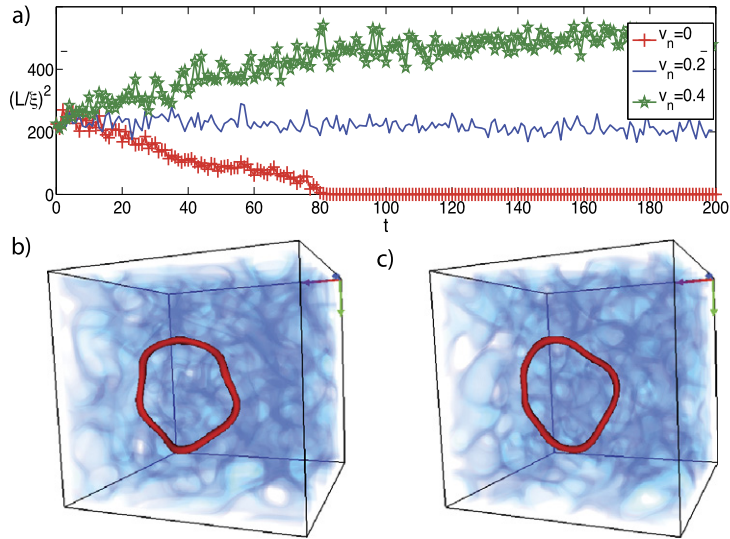


**Fig. 5.** (Color online.) (a) Temporal evolution of the (squared) length of a vortex ring at different values of counterflow  $v_n$  (temperature  $T = 0.4T_\lambda$  and initial radius  $R = 15\xi$ ). (b–c) 3D visualization of vortex ring ( $R = 20\xi$ ) and density fluctuations at  $t = 18, 19$ , with  $T = 0.4T_\lambda$  and resolution  $64^3$ . Thermally-excited Kelvin waves are apparent.

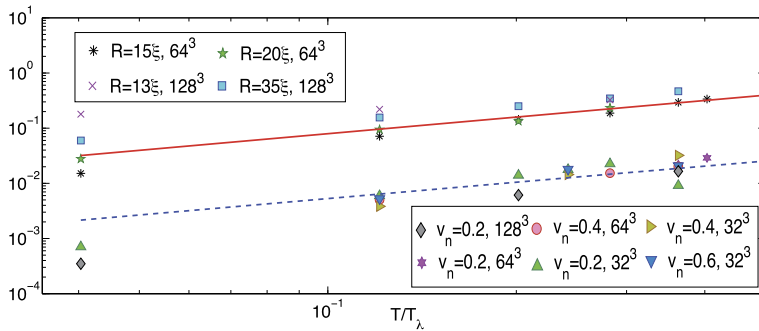


**Fig. 6.** (Color online.) Temperature dependence of counterflow-induced lattice velocity  $v_{\parallel}/v_n$  (bottom) and ring slowdown  $\Delta v_L/u_i$  (top) obtained with  $v_n = 0$ . Dashed line: prediction of Eq. (21) with  $\alpha' = 0.83\rho_n/2\rho$ ; solid line: prediction of anomalous slowdown by Eq. (24) with  $R = 20\xi$  at various resolutions.

Eq. (21) with  $v_n$  perpendicular to the ring and  $v_s = 0$  yields the radial velocity  $\dot{R} = -\alpha(u_i - v_n)$ . The case without counterflow ( $v_n = 0$ ) was studied by Berloff and Youd [32] and a contraction of vortex rings compatible with (21) was reported. To study the influence of counterflow we prepare an initial condition  $\psi = \psi_{\text{ring}} \times \psi_{\text{eq}}$  (with  $\psi_{\text{eq}}$  obtained through Eq. (20)). The temporal evolution of the (squared) vortex length of a ring of initial radius  $R = 15\xi$  at temperature  $T = 0.4T_\lambda$  and  $v_n = 0, 0.2$  and  $0.4$  is displayed in Fig. 5(a). The Berloff–Youd contraction [32] is apparent in absence of counterflow (bottom curve). The temperature dependence of the contraction, related to the  $\alpha$  coefficient in Eq. (21), also quantitatively agrees with their published results (data not shown).

A dilatation of vortex rings is obtained (top curve in Fig. 5(a)) when the counterflow  $v_n$  is large enough. Such a dilatation – a hallmark of counterflow effects – is expected [19] to correspond to a change of sign of  $\mathbf{v}_n - \mathbf{v}_{sl}$  in Eq. (21). However, the predictions of Eq. (21) unexpectedly turn out to be quantitatively wrong. Indeed, using Eq. (22) in the conditions of Fig. 5(a) one finds  $\mathbf{v}_{sl} = \mathbf{u}_i = 0.39$  which is significantly larger than normal velocity  $v_n = 0.2$  around which dilatation starts to take place (see middle curve in Fig. 5(a)). Eq. (21) prediction for the longitudinal velocity  $v_L = (1 - \alpha')u_i + \alpha'v_n$  is also unexpectedly wrong. Using the value of  $\alpha'$  determined in Ref. [18] on the vortex array, one finds  $v_L \sim 0.98u_i$  and from Eq. (22) one finds for  $v_L$  the value  $0.38$  that is larger than the measured value  $v_L = 0.23$ .

This anomaly of the ring velocity  $v_L$  is also present in the absence of counterflow ( $v_n = 0$ ) where Eq. (21) predicts that  $\alpha'$  should be equal to  $\Delta v_L/u_i \equiv (u_i - v_L)/u_i$ . The temperature dependence of  $\Delta v_L/u_i$  is displayed in Fig. 6 (top curve). Observe that  $\Delta v_L/u_i$  is one order of magnitude above the transverse mutual-friction coefficient  $\alpha'$  measured on the lattice of straight vortices.

We now relate the thermally-induced anomaly to the velocity  $v_a$  induced on a vortex ring by a single Kelvin wave of (small) amplitude  $A$  and (large) wavenumber  $N_K/2\pi R$ . Indeed, the presence of a Kelvin wave is known to slowdown the

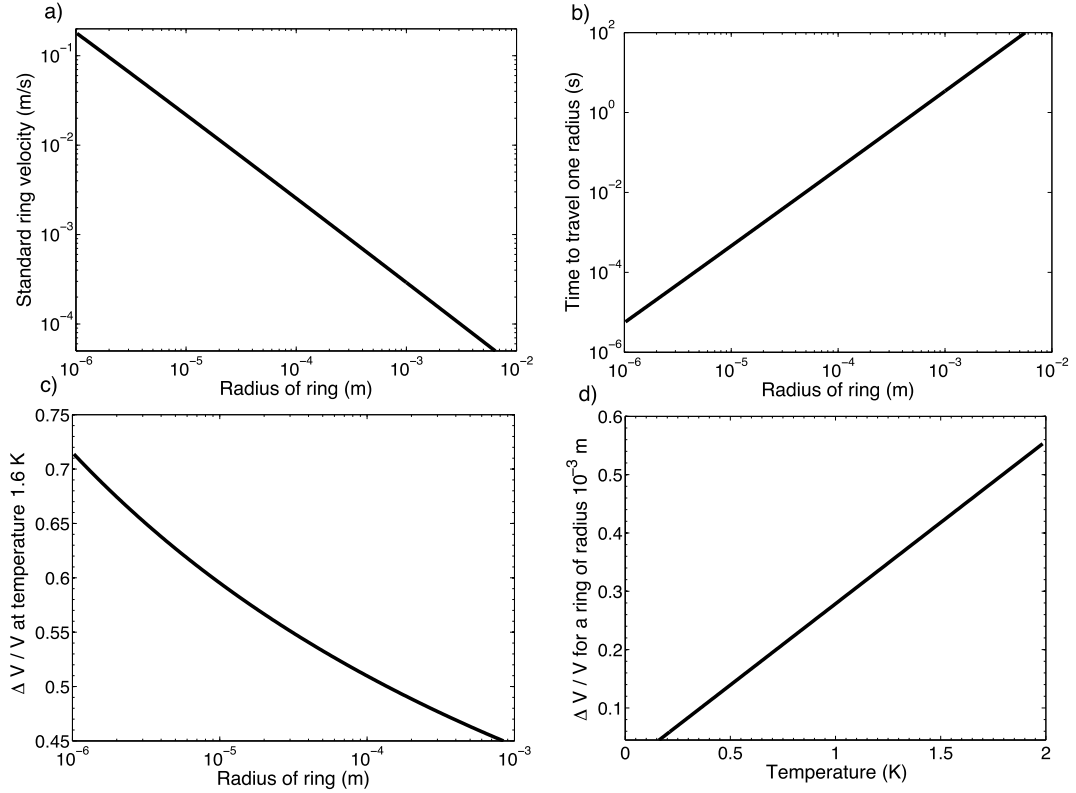


**Fig. 7.** Estimates of ring velocities in  ${}^4\text{He}$  (see text): (a) standard ring velocity  $u_i(R)$ , see Eq. (22), (b) time to travel one radius:  $R/u_i(R)$ , (d) relative anomalous slowdown  $\Delta v_L/u_i$ , see Eq. (24) as a function of the radius at  $T = 1.6$  K and (d) for a ring of 1 mm radius as a function of temperature.

ring, by an amount that was obtained in the LIA [38] and Biot–Savart [39] frameworks. The velocity  $v_a$  reads (see Eq. (26) of [38])

$$v_a = u_i \left( 1 - A^2 N_K^2 / R^2 + 3A^2 / 4R^2 \right) \quad (23)$$

where  $u_i$  is the (undisturbed) ring velocity (22).

The TGPE model naturally contains thermal fluctuations that excite Kelvin waves as apparent from Fig. 5(b–c). We assume that the slowing down effect of each individual Kelvin wave is additive and that the waves populate all the possible modes. Kelvin waves being bending oscillations of the quantized vortex lines their wavenumber must satisfy  $k \leq k_\xi = 2\pi/\xi$ . The total number of thermally-excited Kelvin waves is thus  $\mathcal{N}_{\text{Kelvin}} \approx Rk_\xi$ .

The amplitude term  $A^2 N_K^2 / R^2$  in (23) can be obtained by simple equipartition arguments. The energy of a (perfect) ring is

$$E = \frac{2\pi^2 \rho_s \hbar^2}{m^2} R [C(R/\xi) - 1]$$

with the superfluid density  $\rho_s$  [19]. A Kelvin wave produces a variation of the ring length  $\Delta L = \pi A^2 N_K^2 / R$ . Its energy can thus be estimated as  $\Delta E = \frac{dE}{dR} \frac{\Delta L}{2\pi}$ . Assuming  $\Delta E = \beta^{-1}$  yields, at low temperature where  $\rho_s \approx \rho$ ,  $A^2 N_K^2 / R^2 = m^2 \beta^{-1} / \pi^2 \rho \hbar^2 R C(R/\xi)$ . Replacing  $A^2 / R^2$  in Eq. (23), the dominant effect is obtained by summing up to  $\mathcal{N}_{\text{Kelvin}}$  and it finally reads:

$$\frac{\Delta v_L}{u_i} \equiv \frac{u_i - v_a}{u_i} \approx \frac{\beta^{-1} m^2}{\pi^2 \rho \hbar^2 C(R/\xi)} k_\xi \quad (24)$$

The thermally-induced anomalous slowdown (24) is in good agreement with the TGPE data displayed in Fig. 6.

We now try to estimate the order of magnitude of the effect in liquid  ${}^4\text{He}$ . We use the value 238 m/s for the speed of sound at very low temperatures. The standard values of  $\hbar$  and the atomic mass of  ${}^4\text{He}$  then yield a coherence length of  $\xi_{\text{He}} = 0.47 \times 10^{-10}$  m. This, together with the GPE value of 0.615 for  $a$  (see Eq. (22)) gives the standard velocities of  ${}^4\text{He}$  vortex ring that are displayed in Fig. 7(a–b).

Using the standard values of  $k_B$  and the density of  ${}^4\text{He}$   $\rho_{\text{He}} = 145 \text{ kg/m}^3$  gives the estimates for the slowdown formula (24) that are displayed in Fig. 7(c–d).

A ring of radius 1 mm is seen to travel at only 0.446 of its standard velocity at  $T = 1.6$  K. The slowdown is linear in  $T$  and at  $T = 0$  the standard velocity of a 1 mm ring is 0.29 mm/s. The effect is larger for smaller rings. Note that experimentally *independent* measurements of velocity and radius are needed to detect the effect.

However, note that these estimates are based on (24), a purely classical formula that needs to be extended in order to take into account quantum effects. Indeed, the dispersion relation of Kelvin waves  $\omega(k) = \frac{\hbar}{2m}k^2C(R/\xi)$  [38] implies (using the relation  $\hbar\omega(k_{\text{eq}}) = \beta^{-1} = k_{\text{B}}T$ ) that Kelvin waves are not in equipartition for wavenumbers  $k > k_{\text{eq}} = (2mk_{\text{B}}T/\hbar^2C(R/\xi))^{1/2}$ , as (like in blackbody radiation) quantum effects are relevant in this range.

In the case of weakly-interacting BEC with mean inter-atomic particle distance  $\ell \sim |\hat{\psi}_{\mathbf{0}}|^{-2/3}$  satisfying  $\tilde{a} \ll \ell \ll \xi$  the condensation temperature is  $T_{\lambda} \sim \hbar^2/k_{\text{B}}m\ell^2$ . For  $T > T^*$ , where  $T^*/T_{\lambda} \sim C(R/\xi)\ell^2/\xi^2 \ll 1$ , it is straightforward to show that  $k_{\text{eq}} > k_{\xi}$  and therefore that (24) directly applies and reads  $\Delta v_L/u_i \sim (\ell/\xi)(T/T_{\lambda}C(R/\xi))$ . For  $T < T^*$ ,  $k_{\xi}$  must be replaced by  $k_{\text{eq}}$  in formula (24) and the slowdown becomes  $\Delta v_L/u_i \sim (T/T_{\lambda}C(R/\xi))^{3/2}$ .

Furthermore note that, at zero-temperature, it is natural to suggest that the quantum fluctuations of the amplitudes of Kelvin waves produce an additional effect. This effect can be estimated by using  $\Delta E = \hbar\omega(k)/2$ . It is radius-independent and of order  $\Delta v_L/u_i \sim (\ell/\xi)^3$  (see the discussion following Eq. (91) in Ref. [16]).

In a low- $T$  physical BEC, with quantum distribution of sound waves,  $\rho_n/\rho \sim (T/T_{\lambda})^4$  [22] and the standard effects (21) are of order  $(T/T_{\lambda})^4$ . Thus the new effect should dominate in this limit. In the case of superfluid  $^4\text{He}$  the interaction is not weak and the GPE description is only expected to give qualitative predictions [19]. Nevertheless the new effect should also be dominant at low temperature and Fig. 7(c–d) should give correct orders of magnitude for  $T^* < T < T_{\lambda}$ .

#### 4. Conclusion

The condensation transition observed in Refs. [15,30,31] was shown to correspond to a standard two-component second order phase transitions [33,34] which is the class of the  $\lambda$ -transition of  $^4\text{He}$ . We found that TGPE equilibrium can also be obtained by a direct energy cascade, just like in the truncated Euler equation [10]. Increasing the amount of dispersion of the system a slowdown of the energy transfer was produced inducing a partial thermalization independently of the truncation wavenumber.

Having both the right very low-temperature dynamics and the correct  $\lambda$ -transition it makes sense to check if the TGPE dynamics is consistent with standard mutual-friction phenomenology. We found that the answer was yes, with one exception.

The unexpected result was found by immersing a vortex ring in a finite-temperature bath: a strong dependence of the translational velocity in the temperature was observed. We explained this effect by relating it to the anomalous translational velocity due to finite amplitude Kelvin waves that was previously found by Kiknadze and Mamaladze [38] and Barenghi et al. [39]. Assuming equipartition of the energy of the Kelvin waves with the heat bath yields a formula that gives a very good quantitative estimate of the numerically observed effect. This new formula also gives an experimentally-testable quantitative prediction for the thermal slowdown of vortex rings in superfluid  $^4\text{He}$ .

#### Acknowledgements

The work mentioned in this article was performed in collaboration with M. Abid, C. Cartes, C. Cichowlas, C. Huepe, G. Krstulovic, S. Metens, C. Nore, C.-T. Pham, L. Tuckerman and E. Tirapegui. Computations were performed at the Institut du développement et des ressources en informatique scientifique.

#### References

- [1] M. Abid, C. Huepe, S. Metens, C. Nore, C.T. Pham, L.S. Tuckerman, M.E. Brachet, Gross–Pitaevskii dynamics of Bose–Einstein condensates and superfluid turbulence, *Fluid Dyn. Res.* 33 (5–6) (2003) 509.
- [2] C.T. Pham, C. Nore, M.E. Brachet, Boundary layers in Gross–Pitaevskii superflow around a disk, *C. R. Physique* 5 (1) (2004) 3–8.
- [3] C.T. Pham, C. Nore, M. Brachet, Boundary layers and emitted excitations in nonlinear Schrödinger superflow past a disk, *Physica D* 210 (3–4) (2005) 203–226.
- [4] G. Krstulovic, M. Brachet, E. Tirapegui, Radiation and vortex dynamics in the nonlinear Schrödinger equation, *Phys. Rev. E* 78 (2008) 026601.
- [5] G. Krstulovic, M. Brachet, Comment on “Superfluid turbulence from quantum Kelvin wave to classical Kolmogorov cascades”, *Phys. Rev. Lett.* 105 (2010) 129401.
- [6] T.D. Lee, On some statistical properties of hydrodynamical and magneto-hydrodynamical fields, *Quart. Appl. Math.* 10 (1) (1952) 69–74.
- [7] R. Kraichnan, On the statistical mechanics of an adiabatically compressible fluid, *J. Acoust. Soc. Am.* 27 (3) (1955) 438–441.
- [8] R. Kraichnan, Helical turbulence and absolute equilibrium, *J. Fluid Mech.* 59 (1973) 745–752.
- [9] S.A. Orszag, Statistical theory of turbulence, in: R. Balian, J.L. Peube (Eds.), *Fluid Dynamics, Les Houches, 1973*, Gordon and Breach, New York, 1977.
- [10] C. Cichowlas, P. Bonaiti, F. Debbasch, M. Brachet, Effective dissipation and turbulence in spectrally truncated Euler flows, *Phys. Rev. Lett.* 95 (26) (2005) 264502.
- [11] G. Krstulovic, M. Brachet, Two-flow model of the truncated Euler equations, *Physica D: Nonlinear Phenom.* 237 (14–17) (2008) 2015–2019.
- [12] G. Krstulovic, P.D. Mininni, M.E. Brachet, A. Pouquet, Cascades, thermalization, and eddy viscosity in helical Galerkin truncated Euler flows, *Phys. Rev. E* (May 2009) 1–5.
- [13] G. Krstulovic, C. Cartes, M. Brachet, E. Tirapegui, Generation and characterization of absolute equilibrium of compressible flows, *Int. J. Bifurc. Chaos* 19 (10) (2009) 3445–3459.
- [14] N.P. Proukakis, B. Jackson, Finite-temperature models of Bose–Einstein condensation, *J. Phys. B: At. Mol. Opt. Phys.* 41 (2008) 203002.

- [15] M.J. Davis, S.A. Morgan, K. Burnett, Simulations of Bose fields at finite temperature, *Phys. Rev. Lett.* 87 (16) (2001) 160402.
- [16] G. Krstulovic, M.E. Brachet, Energy cascade with small-scale thermalization, counterflow metastability, and anomalous velocity of vortex rings in Fourier-truncated Gross–Pitaevskii equation, *Phys. Rev. E* 83 (2011) 066311.
- [17] G. Krstulovic, M.E. Brachet, Dispersive bottleneck delaying thermalization of turbulent Bose–Einstein condensates, *Phys. Rev. Lett.* 106 (2011) 115303.
- [18] G. Krstulovic, M.E. Brachet, Anomalous vortex-ring velocities induced by thermally excited Kelvin waves and counterflow effects in superfluids, *Phys. Rev. B* 83 (2011) 132506.
- [19] R.J. Donnelly, *Quantized Vortices in Helium II*, Cambridge Univ. Press, Cambridge, 1991.
- [20] E.P. Gross, Structure of a quantized vortex in boson systems, *Nuovo Cimento* 20 (3) (1961).
- [21] L.P. Pitaevskii, Vortex lines in an imperfect Bose gas, *Sov. Phys. JETP* 13 (2) (1961).
- [22] L. Landau, E. Lifchitz, *Fluid Mechanics*, Pergamon Press, Oxford, 1980.
- [23] M.H. Anderson, J.R. Ensher, M.R. Matthews, C.E. Wieman, E.A. Cornell, Observation of Bose–Einstein condensation in a dilute atomic vapor, *Science* 269 (1995) 198.
- [24] K.B. Davis, M.O. Mewes, M.R. Andrews, N.J. van Druten, D.S. Durfee, D.M. Kurn, W. Ketterle, Bose–Einstein condensation in a gas of sodium atoms, *Phys. Rev. Lett.* 75 (1995) 3969.
- [25] C.C. Bradley, C.A. Sackett, R.G. Hulet, Bose–Einstein condensation of lithium: Observation of limited condensate number, *Phys. Rev. Lett.* 78 (6) (1997) 985.
- [26] F. Dalfovo, S. Giorgini, L.P. Pitaevskii, S. Stringari, Theory of Bose–Einstein condensation in trapped gases, *Rev. Mod. Phys.* 71 (3) (1999).
- [27] Y. Pomeau, S. Rica, Model of superflow with rotons, *Phys. Rev. Lett.* 71 (2) (1993) 247.
- [28] C. Huepe, M.E. Brachet, Scaling laws for vortical nucleation solutions in a model of superflow, *Physica D* 140 (2000) 126–140.
- [29] D. Gottlieb, S.A. Orszag, *Numerical Analysis of Spectral Methods*, SIAM, Philadelphia, 1977.
- [30] C. Connaughton, C. Josserand, A. Picozzi, Y. Pomeau, S. Rica, Condensation of classical nonlinear waves, *Phys. Rev. Lett.* 95 (26) (2005) 263901.
- [31] G. Düring, A. Picozzi, S. Rica, Breakdown of weak-turbulence and nonlinear wave condensation, *Physica D* 238 (16) (2009) 1524–1549.
- [32] N.G. Berloff, A.J. Youd, Dissipative dynamics of superfluid vortices at nonzero temperatures, *Phys. Rev. Lett.* 99 (14) (2007).
- [33] D.J. Amit, *Field Theory: The Renormalization Group and Critical Phenomena*, World Scientific Publishing Company, 2005.
- [34] J. Zinn-Justin, *Phase Transitions and Renormalisation Group*, Oxford University Press, USA, 2007.
- [35] C. Nore, M. Abid, M.E. Brachet, Kolmogorov turbulence in low-temperature superflows, *Phys. Rev. Lett.* 78 (20) (1997) 3896–3899.
- [36] C. Nore, M. Abid, M. Brachet, Decaying Kolmogorov turbulence in a model of superflow, *Phys. Fluids* 9 (9) (1997) 2644.
- [37] J. Salort, P.-E. Roche, E. Leveque, Mesoscale equipartition of kinetic energy in quantum turbulence, *EPL (Europhys. Lett.)* 94 (2) (2011) 24001.
- [38] L. Kiknadze, Y. Mamaladze, The waves on the vortex ring in He II, *J. Low Temp. Phys.* 126 (1–2) (2002) 321–326.
- [39] C.F. Barenghi, R. Hanninen, M. Tsubota, Anomalous translational velocity of vortex ring with finite-amplitude Kelvin waves, *Phys. Rev. E* 74 (4) (2006) 046303.